Cr(III) exchange on zeolites obtained from kaolin and natural mordenite

Cristian Covarrubias [a], Rafael García [a,*], Renán Arriagada [a], Jorge Yánez [a], María Teresa Garland [b]

[a] *Facultad de Ciencias Químicas, Universidad de Concepción, Casilla 160-C, Concepción, Chile*
[b] *Departamento de Física, Facultad de Ciencias Físicas y Matemáticas and CIMAT, Universidad de Chile, Santiago, Chile*

Abstract

Zeolites with high Cr(III) exchange capacity were synthesized from kaolin and natural mordenite. The intermediate phases and final products were characterized by X-ray diffraction, FTIR spectroscopy, scanning electron microscopy, thermogravimetric analysis, N_2-adsorption and chromium exchange capacity (CrEC). In addition, precise zeolitic phases were identified using the TOPAS program based on Rietveld refinement. Hydrothermal synthesis from kaolin leads to the formation of a mixture of zeolites-X and A. At higher hydrothermal treatment period, zeolite-X (space group *Fd-3*) appears as the dominant phase. In the synthesis from natural mordenite a mixture of zeolite-Y (*Fd-3m*) and orthorhombic zeolite-P2 (*Pnma 62*) is formed, obtaining a more pure zeolite-P with the increase in reaction time. The differences in the course of the crystallization/transformation process in both systems are explained in terms of the differences in the dissolution rate of the starting materials in alkaline medium. The CrEC of synthesis products was determined by the type of zeolite and the fraction of amorphous phase in the solid product. It was found that the highest CrEC is obtained for synthesis products containing FAU-type zeolites. The chromium exchange on FAU zeolites is favored due to the larger pore opening, which facilitates the diffusion of large hydrated chromium ions into the internal cation exchange sites. Synthesized zeolite products presented higher Cr(III) exchange capacity than commercial zeolites. These results suggest that the use of these synthesized materials in Cr(III) removal from industrial wastewater could be promising.

Keywords: Zeolite synthesis; Cr(III) exchange; Kaolin; Natural mordenite; Zeolite transformation

1. Introduction

Zeolites are materials widely known for their ion exchange properties [1]. Zeolitic materials are a good example of how the structure at an atomic scale can determine macroscopic properties, and how a detailed knowledge of structure can favor performance prediction. The Si/Al framework ratio of the zeolite determines its maximum ion exchange capacity; however the real capacity may be lower if a proportion of the charge compensation cations are inaccessible for the exchanging ion [2]. The aperture dimensions control exchanging ion entry into zeolite cavities, and may be a limiting factor during the ion exchange process [3]. Chromium (III) has the largest hydrated ionic radius of any known heavy metal [4] and its exchange in zeolitic materials requires a favorable pore opening. The study of the Cr(III) exchange in zeolites is interesting from an environmental point of view: the use of zeolitic materials in the control of pollution has received increasing attention [5–12] due to their good selectivity for cations such as Cr(III) from tannery effluents and the relatively low cost when using zeolite packed beds.

Cr(III) removal using several commercial synthetic and naturally occurring zeolites have been studied in previous

* Corresponding author. Tel.: +56 41 204324; fax: +56 41 245974.
E-mail address: rgarcia@udec.cl (R. García).

works [13–15]. It was found that the commercial synthetic Na-X zeolite exhibits the highest Cr(III) exchange capacity. The structure of faujasite zeolites (natural faujasite and synthetics analogs X and Y) is one of the most open of all zeolites and are composed of significantly large openings of ~0.74 nm. FAU-type zeolites are synthesized from pure reactive, such as solutions of sodium aluminate, sodium silicate, colloidal silica and triethanolamine (TEA). However, when zeolite is used for ion exchange units, it needs to have a competitive price with respect to other ion exchangers, since water purification processes consume large amounts of the exchanger material. For this reason, it is preferable to synthesize zeolites from more economical sources, such as natural aluminosilicates. De Lucas et al. [16] have reported the synthesis of zeolite X from calcined kaolin using silicate solution as an additional silica source and under normal pressure conditions. The variables were optimized to obtain zeolite-X with the established specifications for its use in detergent formulation. Rees and Chandrasekhar [17,18] have studied the formation of zeolite from kaolinite, metakaolinite and sodium aluminosilicate gel, using a sodium hydroxide medium and fluoride-containing medium at autogenous pressure. Kaolinite gave partially rehydrated non-basic hydroxysodalite, whereas zeolite 4A is produced from metakaolinite and sodium aluminosilicate gel. When a fluoride medium was used, kaolinite gave zeolite-P directly without any intermediate meta-stable phase; whereas zeolite-X was the stable intermediate from metakaolinite. The transformation of kaolin to low-silica X zeolite (LSX) was studied by Akolekar et al. [19], where metakaolin is converted to zeolite X plus a small amount of zeolite A in alkaline solution. The amount of zeolite-A decreases with increasing synthesis time, but there is an overall increase in product crystallinity and surface area. Chilean kaolinites have been used for the synthesis of Na-A zeolite with builder properties in powdered detergents [20]. No adverse effects have been found with respect to the presence of abundant coaly matter in the initial materials. Zeolites may also be obtained from starting materials such as volcanic glass [21], diatomite [22] and recently from fly ash [23,24]. Another form of zeolite synthesis is the transformation of one zeolite type into other zeolite types. Some zeolites represent metastable structures that may, under given conditions, be transformed into other more stable phases [2]. Subotić et al. [25] studied the kinetics of the transformation of synthetic zeolite-A into zeolite-P, showing that the processes take place by nucleation and crystal growth of the solution. The transformations of zeolite-X to HS and zeolite Y to P also have been studied [26]. Studies on transformation of well-known natural zeolites, such as mordenite, clinoptilolite or erionite into faujasite, have not been found in the literature. Highly occurring zeolites, such as mordenite and clinoptilolite, could be transformed under specific conditions into faujasite, a zeolite rarely found in nature.

The objective of this work is the synthesis of zeolites with high Cr(III) exchange capacity (CrEC) using kaolin and natural mordenite as starting materials, and to evaluate the effect related to the reaction time on the crystallization/transformation process and on product CrEC. The intermediates phases and final products were characterized by XRD, FTIR, SEM, N_2-adsorption and TG/DTG. Additionally, precise zeolitic phases analyzed by XRD were identified using the TOPAS program based on the Rietveld refinement.

2. Experimental

2.1. Materials

The starting materials used for the synthesis were kaolin (Sigma) and natural mordenite. Table 1 shows the chemical composition of the natural materials obtained by X-ray fluorescence. The mordenite zeolite was obtained from a natural deposit near the locality of Parral, situated about 300 km south of Santiago, Chile. To obtain a more reactive phase, kaolin and natural mordenite were used after calcination at 900 °C for 30 min.

2.2. Experimental

The synthesis experiments were carried out using a reaction mixture with the following molar composition: $3.75Na_2O{:}1.0Al_2O_3{:}2.5SiO_2{:}243.7H_2O$. This reaction mixture was prepared by mixing the calcined starting materials (metakaolin or calcined mordenite) with sodium hydroxide pellets and deionized water in a Teflon vessel (100 ml) at room temperature. The SiO_2/Al_2O_3 ratio of the reaction mixture was adjusted by adding appropriate amounts of sodium metasilicate salt ($Na_2SiO_3 \cdot 5H_2O$, BDH) and aluminiumoxide (Al_2O_3, Merck) for experiments with metakaolin and natural mordenite, respectively. The resulting mixtures were immediately placed in a Teflon-lined stainless steel reactor and kept in an oven for hydrothermal synthesis. The hydrothermal period was carried out at 100 °C under autogenous pressure and static conditions. The influence of the crystallization time on the type of formed

Table 1
Chemical composition of the starting materials (wt.%)

	SiO_2	Al_2O_3	TiO_2	MgO	CaO	Fe_2O_3	Na_2O	K_2O	MnO	Molar SiO_2/Al_2O_3
Kaolin	45.4	38.5	1.60	0.03	0.15	0.50	0.20	0.10	–	2.00
Natural mordenite	70.66	12.69	0.30	0.68	3.35	1.21	1.47	1.10	0.20	9.45

zeolite and the Cr(III) exchange capacity of the products was studied. The synthesis products were obtained after 1, 5, 15, 48, 96, 120 and 240 h of the crystallization. After completion of the synthesis period, the product was filtered, washed and dried overnight at 100 °C.

2.3. Cr(III) exchange capacity (CrEC)

These assays were carried out by placing 0.4 g of synthesized product in contact with 80 ml of Cr(III) solution (500 mg/l), which was prepared from the basic salt chromium sulfate $Cr(OH)SO_4 \cdot Na_2SO_4$, a salt commonly used in the tannery processes. According to a previous study on the exchange rate of Cr(III) in zeolites [16], the chromium exchange assay was achieved after 24 h in a thermostatic bath at 25 °C under continuous agitation. The chromium concentrations in the starting solution and filtered solution were measured using a Perkin–Elmer Analyst 100 atomic absorption spectrophotometer (AAS). The Cr(III) exchange capacity of the commercial zeolites 13X (BDH Chemicals Ltd.), 4A (Union Carbide Corp.) and Na-Y (Strem Chemicals) were used as references.

2.4. Characterization

The zeolitic phases in synthesis products were identified using X-ray diffraction (XRD). Powder X-ray diffraction patterns were measured on a Siemens D 5000 diffractometer using CuKα radiation within a 2θ range of 5–50° with a scanning speed of 1.2°/min. Additionally, the TOPAS software [27] was used in order to determine the precise zeolitic phase. TOPAS is an indexing program based on Rietveld refinement. The Rietveld method using TOPAS requires crystallographic information as approximate cell parameters of the structure, rough knowledge about the cell content (e.g. chemical elements, amount of formula units in cell (density), molecule fragments) and a space group guess. The indexing was carried out for selected powder diffraction patterns, according to the synthesis product purity. Infrared spectroscopy (FTIR) was used to complement the XRD identification of zeolites types. IR transmission spectra were obtained from KBr disks (1 wt.%) using a Nicolet Magna IR 550 spectrometer.

Zeolite crystal morphology was examined using a scanning electron microscopy (SEM) with an Autoscan microscope. Textural characterization was carried out by N_2 adsorption at 77 K in a Micromeritics Gemini 2370 sorptometer. Apparent specific surfaces areas (S_g) were calculated applying the BET equation to the experimental data obtained from N_2 isotherms.

The starting materials and synthesized products were analyzed by thermogravimetry. The TG/DTG curves were obtained using a Mettler Toledo TG/SDTA851 thermogravimetric analyzer, at heating speeds of 10 °C/min. Air atmosphere was used for kaolin and natural zeolite, similar to the calcination conditions. For the zeolite samples an inert atmosphere of N_2 was used.

3. Results and discussion

3.1. X-ray diffraction

Fig. 1 shows the XRD patterns of kaolin, metakaolin and synthesis products. The transformation from kaolin to metakaolin is completely consistent with the previous literature on the kaolin–metakaolin transformation. Metakaolin is X-ray amorphous; the peaks remaining in the diffraction pattern can be attributed to a mica impurity. It can be observed that the crystallization of zeolitic phases begins from an amorphous gel formed after 1 h of hydrothermal treatment. The XRD patterns show that after 5 h of reaction faujasite and zeolite-A phases will be to crystallize simultaneously. As the reaction progresses, faujasite seems to be the prominent phase, which can be observed by the increase in the intensity of the characteristic FAU peaks at 6.12° and 15.51°, as well as by a reduction in the intensity of the zeolite-A peak at 16.21°. The formation of pure, well-crystallized hydroxysodalite after a long reaction time is also observed. Hydroxysodalite is a condensed phase, and thermodynamically it is the most stable phase formed from the Na_2O–Al_2O_3–SiO_2–H_2O quaternary system. These synthesis products illustrate Oswald's rule of successive transformations, which states that in the formation of polymorphs from vapor, liquid, or solution, the first polymorph to appear is the least thermodynamically stable and it is successively replaced by more stable forms [28]. On the other hand, X-ray analysis of natural mordenite (Fig. 2), shows that zeolite mordenite is accompanied by a small fraction of clinoptilolite, although mordenite is the predominant phase. In contrast with kaolin, the crystalline structure of mordenite is stable after calcination at 900 °C for 30 min, and characteristic XRD peaks of mordenite can be seen even after 1 h of hydrothermal treatment. If the reaction is continued for 5 h, the disappearance of characteristic mordenite peaks can be observed: the peak of mordenite at 6.58° 2θ shifts to 6.22° 2θ, indicating the formation of faujasite phase. Additionally, the XRD peaks at 26.66° 2θ and 28.04° 2θ suggest the presence of zeolite-P. Thus, the solid product obtained at 5 h of reaction would consist of a mixture of amorphous phase, faujasite and zeolite-P. After 15 h of reaction, a more complete crystallization of zeolites FAU and P occurs in the reacting medium. The presence of the faujasite phase in the reaction product can be observed up to 96 h of reaction. As the reaction time advances, zeolite-P appears as the predominant structural phase, and is obtained as pure phase at 120 h of reaction, as judged by the absence of the FAU diffraction peak at 6.12° 2θ. At a longer crystallization time, zeolite-P begins to undergo reconversion to hydroxysodalite, the most condensed, stable structure [29].

The TOPAS software was used to identify the precise zeolite phase for FAU and GIS zeolite frameworks. Refinement analyses were carried out using space groups and crystallographic information obtained from *collection of simulated XRD patterns for zeolites* (*IZA structure commission*) [35].

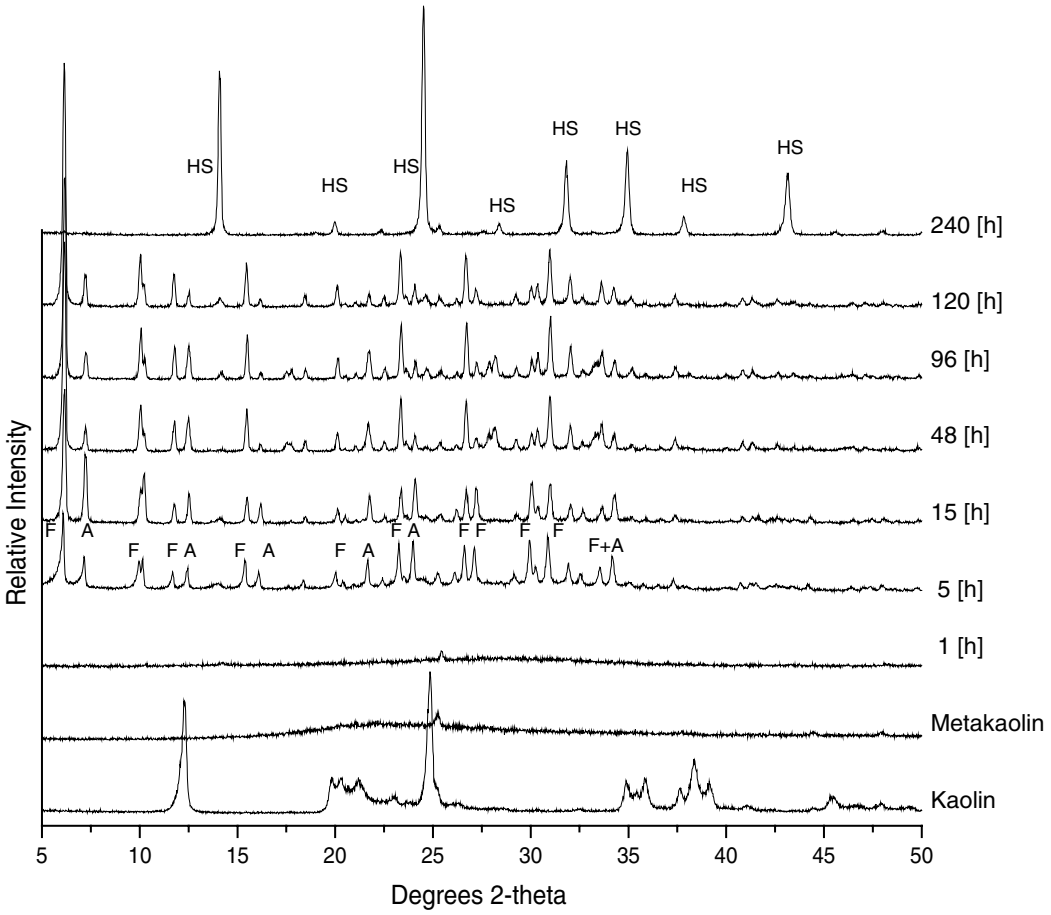

Fig. 1. X-ray diffractograms of kaolin, metakaolin and synthesis products.

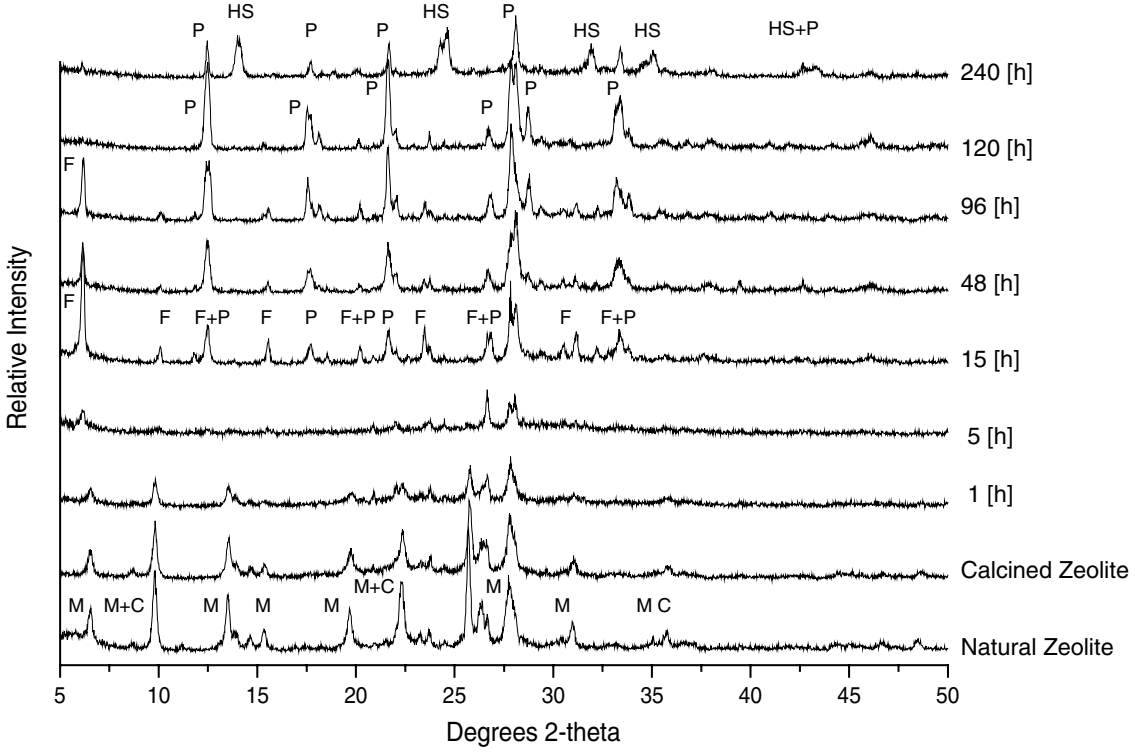

Fig. 2. X-ray diffractograms of natural zeolite, calcined zeolite and synthesis products.

Table 2
Summary of refinement results and identified zeolite phase

	Space group	*a*	*b* (Å)	*c*	Cell vol (Å^3)	R_{Bragg}	Zeolite phase
Product from kaolin (120 h)	*Fd-3*	25.00	–	–	15,625.00	19.341	Na-X
Product from mordenite (15 h)	*Fd-3m*	24.62	–	–	14,923.28	12.946	Na-Y
Product from mordenite (120 h)	*Pnma 62*	9.80	10.03	10.60	1041.91	3.910	P2

Table 2 shows the results for the refinement and the identified zeolite phases for selected metakaolin (120 h) and natural mordenite (15 h and 120 h) products. The space groups *Fd-3* and *Fd-3m* were consistent with the XRD patterns for the FAU zeolite phases synthesized from metakaolin and mordenite, respectively. According to the XRD collection data, the FAU zeolite obtained from metakaolin corresponds to a zeolite Na-X and the FAU zeolite obtained from mordenite suggests a zeolite Na-Y, as judged by its unit cell dimension (24.62 Å) [30]. On the other hand, zeolite-P refinement was consistent with orthorhombic crystal system and space group *Pnma 62*. This zeolitic phase corresponds to a zeolite-P2, which is topologically related to the natural zeolite called gobbinsite [31] and has been identified as a medium-silica P [32]. Even though zeolite-P can appear as an undesirable product during the synthesis of high purity FAU, zeolite-P possesses a high affinity for metallic ions and its efficiency in metallic cation removal has been demonstrated [33].

Assessment of the fit between the calculated and observed data is informed by TOPAS through the R_{Bragg} value, which is closely related to the conventional *R*-values from single crystal refinements [34]. The FAU R_{Bragg} values were higher than those obtained for zeolite P refinement. This difference can be explained by fractions of others zeolitic phases in analyzed products (A and P zeolites). These phases are not considered during the refinement process, which produce an increase in R_{Bragg} values. Fig. 3 shows the Rietveld plots for the synthesis product from mordenite at 120 h of reaction. Due to the higher purity of the zeolite-P product, this sample presented the best agreement between the calculated and observed profiles.

3.2. FTIR spectroscopy

The mid-infrared region contains the fundamental vibrations of the Si, AlO_4 or TO_4 units in zeolite frameworks and, therefore, it contains useful information on the structural characteristics of the zeolite frameworks [35]. Figs. 4 and 5 show the FTIR profiles of the starting materials and synthesis products as a function of reaction time. Kaolin and metakaolin show the characteristic bands as reported in the literature [36], due to Si–O, Si–O–Al, and Al–OH vibrations. The conversion of kaolin to metakaolin can be observed in the loss of Al–OH bands (914 and 1001 cm^{-1}), changes in the Si–O stretching bands, and the disappearance of Al–O–Si bands at 789 and 754 cm^{-1} due to the distortion of the tetrahedral and octahedral layers. These changes are similar to those reported by Akolekar et al. [19]. The most important spectral frequencies

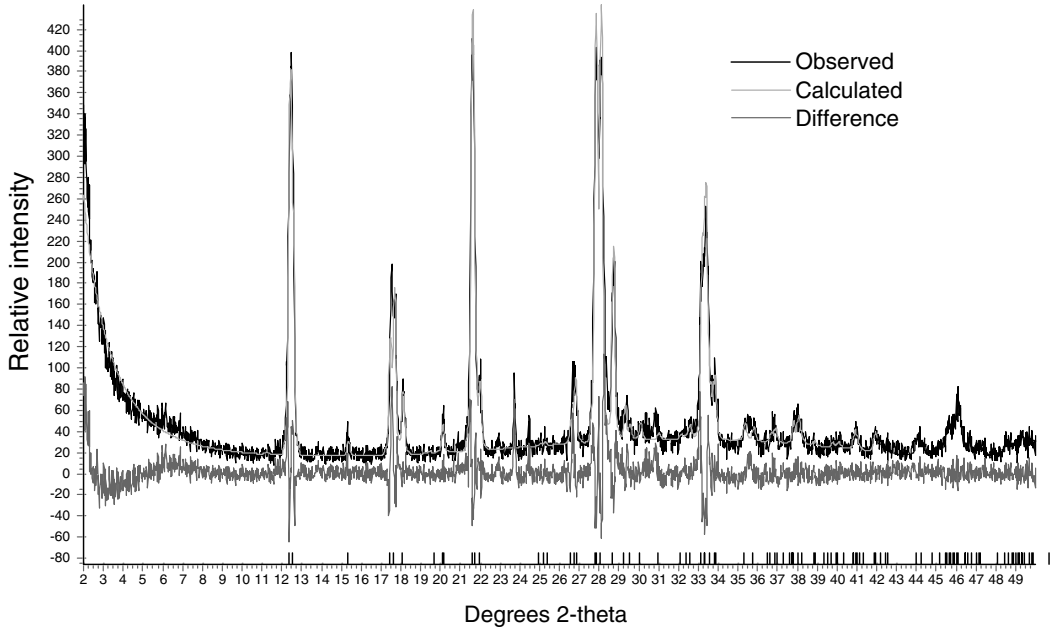

Fig. 3. Rietveld plot of synthesis product from mordenite after 120 h reaction. Observed and calculated diffractions patterns are shown with difference curve below.

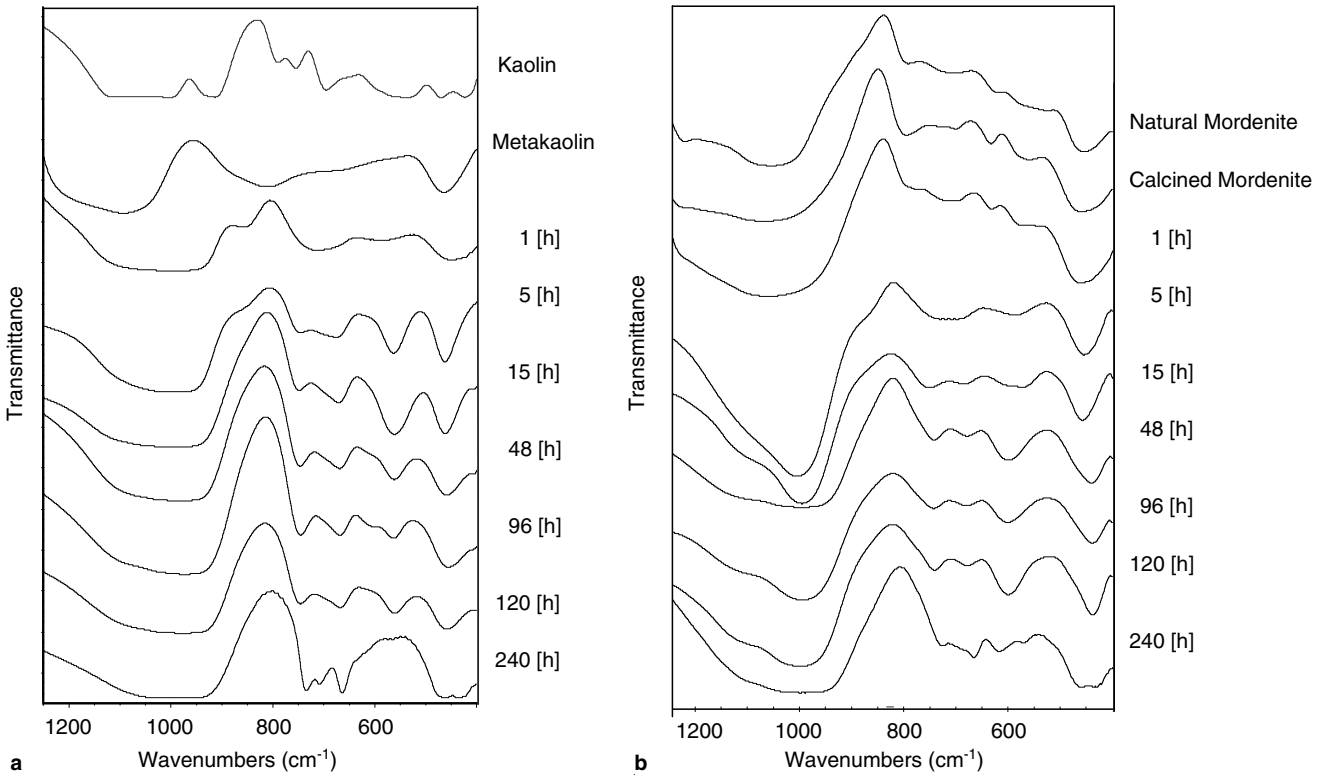

Fig. 4. FTIR spectra of (a) kaolin, metakaolin and synthesis products and (b) natural zeolite, calcined zeolite and synthesis products.

observed on the synthesis products and zeolite references [37] are given in Tables 3 and 4. The characteristic bands of metakaolin disappear after 1 h of reaction, and the new bands at 448, 587, 712, 857 and 922 cm^{-1} become prominent. These bands are of low intensity and have been attributed to the formation of sodium aluminosilicate gel [17]. The bands at 462, 562, 748 and 994 cm^{-1} confirm the formation of faujasite and zeolite-A at 5 h of reaction. The band at 562 cm^{-1} is close to the typical IR band of zeolite-X at 560 cm^{-1} assigned to the double-ring vibration (D6), while bands at 462 and 994 cm^{-1} are close to the bands at 464 cm^{-1} and 995 cm^{-1} corresponding to the internal linkage vibrations of the TO_4 tetrahedra and to the asymmetric stretching of zeolite-A structure, respectively. As the reaction proceeds, bands at 459, 668 and 971 cm^{-1} indicate that Na-X zeolite becomes the prominent phase. The IR frequencies of the final products after 48, 96 and 120 h of reaction are all typical of those of zeolite X used as reference. The formation of pure HS after 240 h can also be observed in the disappearance of the double-ringed band (560 cm^{-1}) and the presence of the characteristic weak bands at 459 and 430 cm^{-1}. These FTIR results are in good agreement with those obtained from the XRD data. On the other hand, IR spectra of the synthesis products from natural mordenite show that calcination and the first hours of hydrothermal treatment produce only slight changes in the mordenite bands. These observations show the high thermodynamical stability of natural zeolite. Characteristic bands of faujasite can be seen after 15 h of reaction. In this case, faujasite bands are closer to those of zeolite-Y than to zeolite-X, which was also suggested by the refinement analysis. As the reaction time increases, a striking change emerges, consisting of the immediate shift of the double-ring vibration of faujasite from 576 cm^{-1} to 599 cm^{-1} after 48 h. This shift reveals the formation of zeolite-P, which is the dominant phase until 120 h of hydrothermal synthesis. After 240 h of reaction, the changes on the T–O bend (436 cm^{-1}) and symmetric T–O stretch (740–677 cm^{-1}) bands, as well as the appearance of new bands at 458–435 cm^{-1} and 725–664 cm^{-1}, confirm the formation of hydroxysodalite phase after more prolonged hydrothermal treatment.

3.3. Scanning electron microscopy

The morphology of the starting materials and chosen synthesis products were examined using SEM. Fig. 5a shows the SEM image of a metakaolin sample, in which it can be observed to metakaolin as an amorphous material, accompanied of some deformed pseudo-hexagonal platelets of initial kaolin. Fig. 5b shows that the zeolite crystals obtained after 15 h of hydrothermal treatment are accompanied by considerable amount of amorphous material, and the crystals of zeolites FAU and A cannot be easily distinguished. However the finding of agglomerated cubic crystals in another zone of the sample (Fig. 5c) reveals the presence of typical zeolite-A crystals. After 120 h of hydrothermal treatment, a more complete

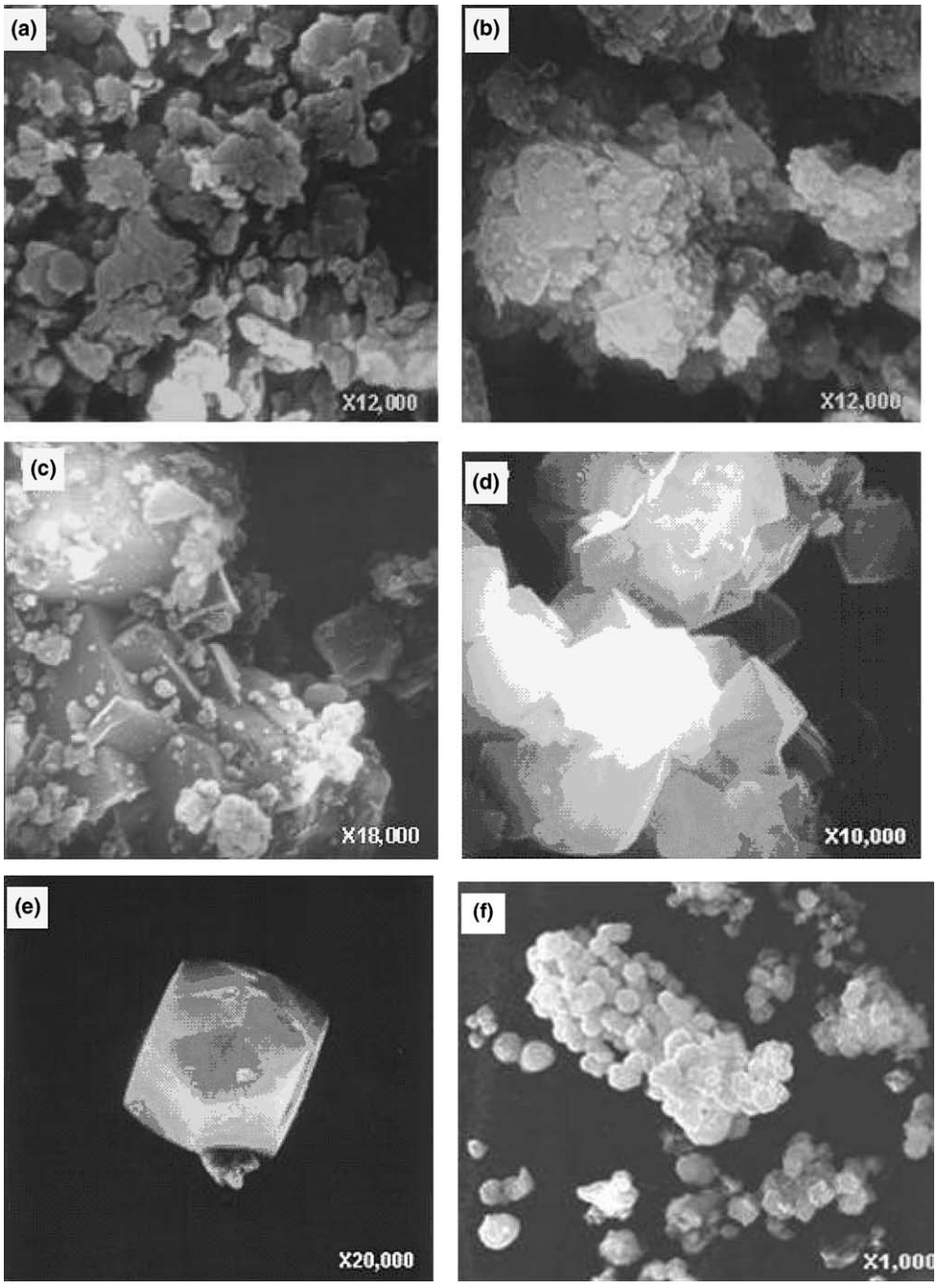

Fig. 5. SEM images of (a) metakaolin, synthesis products after (b, c) 15 h, (d, e) 120 h and (f) 240 h of reaction.

crystallization is observed, and characteristic bipyramidal-shaped crystals of FAU zeolite can be seen (Fig. 5d and e). These well-shaped bipyramidal FAU crystals are not commonly observed in the reported synthesis from natural kaolin [19–22]. Cubic crystals of zeolite were not found in the analyzed sample, which confirms that FAU zeolite is the predominant phase formed at 120 h of hydrothermal treatment. A sample of pure hydroxysodalite obtained after 240 h of crystallization is shown in Fig. 5f. The truncated bipyramidal morphology of this zeolite is frequently observed as spherical entities according to the resolution of SEM microscopy. On the other hand, the observation of a sample of natural calcined zeolite reveals the presence of fibers characteristic of mordenite zeolite (Fig. 6a). Moreover, thin, tabular euhedral crystals of clinoptilolite zeolite [38] were also found in this sample (Fig. 6b). Fig. 6c shows mordenite fibers beside the clinoptilolite crystals in another zone of the analyzed sample. When this natural calcined zeolite is hydrothermally treated for 15 h, faujasite crystal aggregates can be observed on the sample (Fig. 6d). The initial tabular euhedral crystals of clinoptilolite were also found in another zone of the analyzed sample (Fig. 6e),

Table 3
Infrared assignments of synthesis products from kaolin and reference zeolites

	Synthesis products							Zeolites of Ref. [40]		
	1 (h)	5 (h)	15 (h)	48 (h)	96 (h)	120 (h)	240 (h)	X–Y	P	HS
T–O bend (cm^{-1})	459 ms	453 ms	456 ms	439 ms	437 m	436 m	458 ms 435 ms	458 m (X) 456 m (Y)	435 ms	461 ms 432 ms
Double rings (cm^{-1})	568 vw	585 w	576 m	599 m	599 m	598 m	617 ms 570 m	560 m (X) 575 m (Y)	600 m	
Symmetric stretching (cm^{-1})	770 vw 705 w 629 mw	705 w	747 m 687 m	741 ms 677 ms	740 m 677 m	740 m 677 m	725 m 664 m	668 m (X) 746 m 686 m (Y) 784 m	738 ms 670 ms	729 m 660 m
Asymmetric stretching (cm^{-1})	1085 s	1005 s	995 s	995 s	994 s	998 s	997 s	971 (X) 1005 m (Y)	995–1000 s	986 s

Table 4
Infrared assignments of synthesis products from natural mordenite and reference zeolites

	Synthesis products							Zeolites of Ref. [40]		
	1 (h)	5 (h)	15 (h)	48 (h)	96 (h)	120 (h)	240 (h)	X–Y	P	HS
T–O bend (cm^{-1})	459 ms	453 ms	456 ms	439 ms	437 m	436 m	458 ms 435 ms	458 m (X) 456 m (Y)	435 ms	461 ms 432 ms
Double rings (cm^{-1})	568 vw	585 w	576 m	599 m	599 m	598 m	617 ms 570 m	560 m (X) 575 m (Y)	600 m	
Symmetric stretching (cm^{-1})	770 vw 705 w 629 mw	705 w	747 m 687 m	741 ms 677 ms	740 m 677 m	740 m 677 m	725 m 664 m	668 m (X) 746 m 686 m (Y) 784 m	738 ms 670 ms	729 m 660 m
Asymmetric stretching (cm^{-1})	1085 s	1005 s	995 s	995 s	994 s	998 s	997 s	971 (X) 1005 m (Y)	995–1000 s	986 s

which suggests that the dissolution rate of clinoptilolite is considerably lower than that of mordenite zeolite. Fig. 6f shows the SEM image of the sample of zeolite-P obtained after 120 h of reaction. The zeolite-P micrograph can be described as an aggregate of very small particles. Similar aggregates of zeolite-P particles have been obtained from the transformation of zeolite-A into P [26] and by crystallization of zeolites from glass [39]. In this micrograph, clinoptilolite euhedral crystals can be still seen, confirming the slow dissolution of the clinoptilolite crystals in the alkaline medium. This fact would indicate that the crystallization of zeolites FAU and P occurs mainly from mordenite phase, and could explain the differences in the course of the crystallization/transformation process from kaolin (zeolites X, A and HS) and natural zeolite (zeolites Y, P and HS). The low dissolution rate of clinoptilolite may contribute to modify the adjusted composition of the reactant system. Thus, a richer silica gel is probably formed from natural zeolite, which favors zeolite-Y crystallization, as have been already suggested by XRD and FTIR data. The crystallization of zeolite-P from natural zeolite system may also be favored by this change in the gel molar composition. It has been found that the appearance of the zeolite-P phase coincides with an increase in the Si/Al molar ratio of the liquid phase [40]. Zeolite-P is also commonly formed during the synthesis of high-silica faujasite (Na-Y) from aluminosilicates [41]. It has been found that the type of zeolite formed depends upon the nature of the raw material used even when the same molar composition is maintained in the Na_2O–Al_2O_3–SiO_2–H_2O quaternary system [20]. At a given temperature, the course of the crystallization/transformation process depends on the distribution of silicate, aluminate and/or aluminosilicates anions in the liquid phase, which is determined by the silicon and aluminum concentration at given alkalinity [42]. In this study, the alkalinity of the solution was maintained constant ($Na_2O/H_2O = 65$) in both assayed systems, thereby the differences in the concentration of silicon and aluminum species given by the differences in the dissolution rate of metakaolin, mordenite and clinoptilolite crystals in alkaline medium appear to be the main factor that determines the course of the crystallization/transformation process.

3.4. Thermogravimetry (TG/DTG)

TG/DTG curves of starting kaolin are presented in Fig. 7, where it can be seen that kaolin exhibits a clear weight loss within the 450–650 °C temperature range. This event is associated with the dehydroxylation of the aluminosilicate lattice leading to the formation of metakaolin.

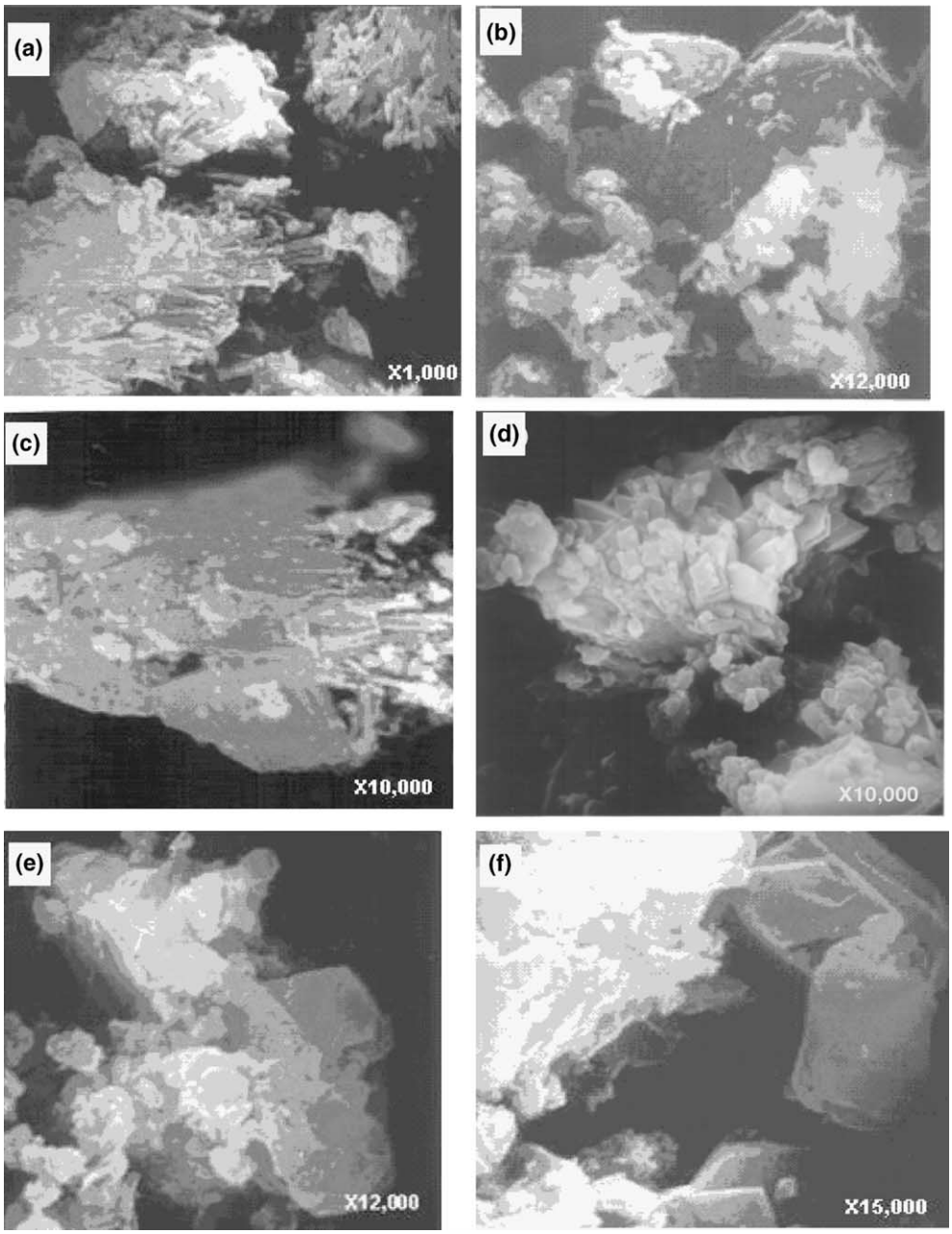

Fig. 6. SEM images of (a)–(c) calcined natural zeolite, synthesis products after (d, e) 15 h and (f) 120 h of reaction.

DTG curves obtained for zeolite products and starting mordenite are shown in Fig. 8 and the characteristic DTG peaks are presented in Table 5. The DTG peaks observed within the 100–143 °C temperature range correspond to the zeolite dehydration steps. The synthesized zeolites present one dehydration step, whereas two dehydration steps are observed for natural zeolite. The position of these DTG peaks as well as the number of dehydration steps [43] can be attributed to the different compensating cation–water binding energies as well as to the different energy associated with the diffusion of the desorbed water through the different zeolite channel systems. Additionally, some zeolites also exhibited DTG peaks after 234 °C, which are assigned to the dehydroxylation steps of the zeolite structure. These weight losses were especially notable for hydroxysodalite and zeolite-P, which are phases obtained after prolonged hydrothermal treatment, and thereby the surface concentration of hydroxyl groups could be higher. Spectroscopic and thermal studies have also demonstrated that OH groups of hydroxysodalite zeolite are exceptionally stable during thermal treatment [44]. Table 5 also shows the weight loss percentages for each zeolite sample, which are produced mainly due to water loss from the zeolite structure. The amount of desorbed water is related with the number of compensation cations in the zeolite structure. It can be seen that the X + A zeolite product obtained from kaolin exhibits the highest weight loss. Zeolites-X and A have a higher amount of cationic

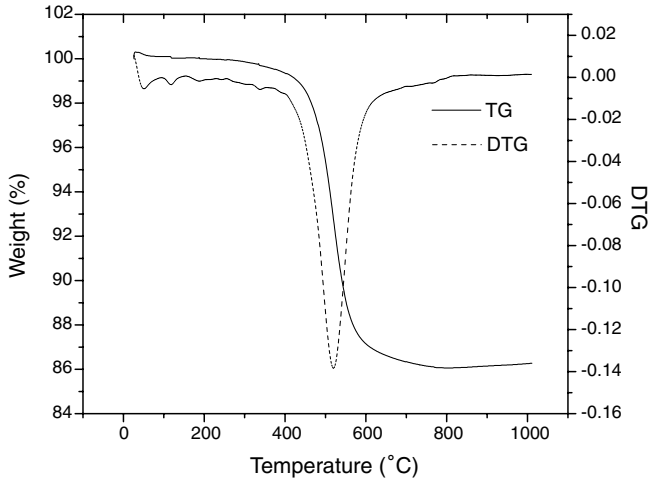

Fig. 7. TG/DTG curves of starting kaolin.

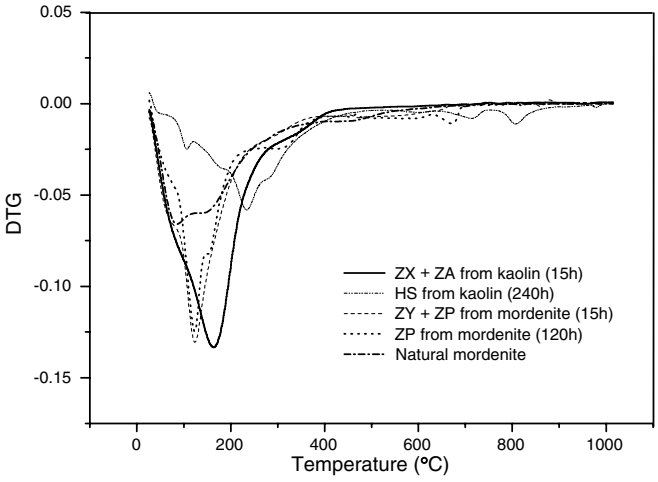

Fig. 8. DTG curves of zeolitic phases.

sites due to their low Si/Al ratio (1.0–1.5), and consequently their water content is higher. Mordenite, due to its high Si/Al ratio (9.7), presents a lower weight loss as well as the P and Y zeolite products, which are also zeolites of higher silicon content. On the other hand, the weight loss exhibited by zeolite HS is lower than those observed for zeolites FAU, A and P; which is in agreement with the accepted zeolite dehydration behavior [45].

3.5. Chromium exchange capacity of synthesized zeolite products

The CrEC of the starting materials, synthesized zeolites and commercial zeolites are presented in Table 3. It can be observed that the highest CrEC was obtained for synthesis products containing FAU-type zeolites (X and Y zeolites). It is known that the maximum ion exchange capacity of the zeolites depends on the number of cation exchange sites, which is determined by the framework Si/Al ratio. However, in previous work [14,46] it was found that in the case of Cr(III) exchange, the zeolite pore opening plays an important role in determining the actual CrEC of the zeolites. Cr^{3+} possesses the largest number of tightly bound water molecules (or the apparent dynamic hydration number, $ADHN = 9.59 \pm 0.31$) [47] and the largest hydrated ionic radius (0.461 nm) for the known heavy metals [4]. Thus, the 12-member rings (with an approximate diameter of 0.74 nm) favor chromium exchange on zeolites-X and Y, and chromium ions can replace a larger amount of compensation cations within zeolite cavities. The CrEC of synthesis products containing X-type zeolite was higher than for those containing Y-type zeolite. Topologically, zeolites-X and Y have a similar aluminosilicate framework structure, although they have different cation position, cation distribution, framework charge, and Si/Al ordering. Zeolite-X has a lower Si/Al ratio and thereby this zeolite exhibited a higher chromium exchange capacity. Additionally, the CrEC of the synthesis products is affected by the presence of another zeolite phase as well as the amorphous phase fraction. It can be observed that the presence of zeolite-A in synthesis products obtained from kaolin seems to increase the CrEC values. Zeolite-A possesses a high cation population due to its low Si/Al ratio (~1.0), and the main access to those cations is through an 8-ring window with an aperture dimension of 0.42 nm. Although large, the chromium ion is polarizable and may pass through the 8-ring apertures. The high-charge framework in zeolite-A is sufficient to deform the cation, permitting the occupation of the internal cation exchange sites [45]. On the other hand, the presence of zeolite P in synthesis products decreases the CrEC values. Zeolite-P (GIS) possesses a higher Si/Al (1.5–2.5) framework than zeolite-A, and thereby exhibits a lower CrEC. In addition, zeolite-P as well as zeolite-A possess a 8-ring pore system. However, the 8-ring apertures in zeolite P are distorted and the free aperture values are

Table 5
DTG peaks and weights loss for zeolite products and naturals mordenite

	DTG peaks (°C)				
	T_1	T_2	T_3	T_4	Weight loss (%)
X + A from kaolin (15 h)	164.4				21.38
P from mordenite (120 h)	122.3	311.1	670.3		18.08
Y + P from mordenite (15 h)	123.4				17.03
Natural mordenite	83.7	143.9			14.37
HS from kaolin (240 h)	104.8	234.9	713.8	806.6	12.46

0.31×0.44 nm and 0.28×0.48 nm [48]. Thus, zeolite-P is formed by more narrow pore apertures (kinetic diameter 0.26 nm) [45], which could also contribute to the lower CrEC observed for this zeolite. The CrEC of zeolite-P (3.01 meq/g) is an important value when compared with commercial zeolite-A. Recent research [24] has also demonstrated that the cation retention capacity of zeolite-P is even higher than for the commercial exchangers such as Amberlite IRC-50. These results suggest that the zeolite-P obtained from natural mordenite could also be efficiently used in water treatment applications. On the other hand, hydroxysodalite presented the lowest CrEC value, as a consequence of their narrow 6-ring apertures (0.22 nm). However hydroxysodalite as well as zeolite A possesses a Si/Al $\sim$ 1, and thereby a high charge density able to polarize the hydrated chromium ion and allow its diffusion through the 6-ring apertures. Table 6 also shows the BET apparent surface area (S_g) calculated from N_2 adsorption isotherms. As can be observed, the highest S_g values are obtained for FAU containing products (304–436 m^2/g). The low S_g values obtained for zeolite-P and hydroxysodalite (59 m^2/g and 10 m^2/g) are a consequence of diffusion restrictions produced under nitrogen adsorption analysis in narrow pore zeolites (<0.4 nm) [49]. The nitrogen molecule has a kinetic diameter of 0.364 nm and its access to the internal pore volume of zeolite-P and hydroxysodalite through narrow opening apertures is limited. This effect has been also previously observed for A-type zeolites [37]. In this case the S_g value for zeolite-4A (0.4 nm) was of 9.4 m^2/g, while for zeolite-5A (0.5 nm) a S_g value of 568 m^2/g is obtained. These observations also provide further evidence on the differences in pore aperture of the synthesized zeolite structures. On the other hand, as previous studies [16,37] have found, natural mordenite presents low CrEC (0.21 meq/g) due to its high Si/Al ratio and the presence of non-zeolitic phases commonly found in the mineral. However, the results of this research demonstrate that natural mordenite, an abundant and low-cost material, can be transformed into zeolites with a high chromium exchange capacity, under controlled hydrothermal conditions.

Table 6
Chromium exchange capacity and specific surface area of starting materials, synthesis products and zeolites of reference

	CrEC (meqCr(III)/g)	S_g (m^2/g)
Starting materials		
Kaolin	0.15	15
Natural mordenite	0.21	277
Synthesis products		
X + A from kaolin (15 h)	4.10	304
X + A from kaolin (120 h)	3.63	436
Y + P from mordenite (15 h)	3.83	316
P from mordenite (120 h)	3.01	59
HS from kaolin (240 h)	2.01	10
Commercial zeolites		
Z13X	3.52	578
ZY	2.08	630
Z4A	3.05	9.4

4. Conclusions

Zeolites with high CrEC can be synthesized using kaolin and natural mordenite as initial materials. Hydrothermal synthesis from kaolin leads to the formation of a mixture of zeolites-X and A in a short reaction time, and zeolite-X may be obtained as a prominent phase with a higher hydrothermal treatment period. In the synthesis from natural mordenite, a mixture of zeolite-Y and P is obtained, and a purer zeolite P is obtained with the increase of reaction time. In both assayed systems, hydroxysodalite was formed as the most thermodynamically stable phase after prolonged hydrothermal treatment. The differences in the course of the crystallization/transformation process can be explained in terms of the differences in the concentration of silicon and aluminum species in the liquid phase, given by the differences in the dissolution rate of metakaolin, mordenite and clinoptilolite crystals in alkali medium. The Cr(III) exchange capacity of synthesis products was determined by the type of zeolite, its Si/Al ratio and pore opening as well as by the fraction of amorphous phase in the solid product. It was found that the highest CrEC was obtained for synthesis products containing FAU-type zeolites. The chromium exchange on FAU zeolites is favored by the larger pore opening, which facilitates the diffusion of large hydrated chromium ions into the internal cation exchange sites. Synthesized zeolites products presented higher Cr(III) exchange capacity than commercial zeolites. These results make the synthesized materials promissory for use in Cr(III) removal from industrial wastewater.

Acknowledgment

The authors wish to thank CONICYT for the Doctorate Scholarship (C. Covarrubias) and the MECESUP-red UCH0116 Project for financial assistance in X-ray analysis.

References

[1] G. Gianneto, A. Montes, G. Rodríguez, Zeolitas Características, Propiedades y Aplicaciones Industriales, Innovación Tecnológica, Facultad de Ingeniería—UCV, Caracas, 2000, p. 305.
[2] A.K. Cheetman, P. Day, Solid State Chemistry Compounds, Oxford University Press Inc., New York, 1992, p. 266.
[3] L. Smart, E.E. Moore, Solid State Chemistry an Introduction, Addison-Wesley Iberoamericana, Wilmington, Delaware, 1995, p. 198.
[4] E.R. Nightingale Jr., Phys. Chem. 63 (1959) 1381.
[5] S. Chen, K. Chao, T. Lee, Ind. Eng. Chem. Res. 29 (1990) 2020.
[6] M. Pansini, C. Colella, M. Gennaro, Desalination 83 (1991) 45.
[7] M.A. Keane, Micropor. Mater. 3 (1995) 93.
[8] B. Biškup, B. Subotić, Sep. Sci. Technol. 33 (4) (1998) 449.
[9] B. Biškup, B. Subotić, Sep. Sci. Technol. 35 (14) (2000) 2311.
[10] J.S. Kim, M.A. Keane, J. Chem. Technol. Biotechnol. 77 (2002) 633.

[11] M.A.S.D. Barros, A.S. Zola, P.A. Arroyo, E.F. Sousa-Aguiar, C.R.G. Tavares, Braz. J. Chem. Eng. 20 (2003) 413.
[12] R. Petrus, J. Warchol, Micropor. Mesopor. Mater. 61 (2003) 137.
[13] M.A.S.D. Barros, N.R.C.F. Machado, F.V. Alves, E.F. Sousa-Aguiar, Braz. J. Chem. Eng. 14 (1997) 104.
[14] R. García, R. Cid, R. Arriagada, J. Soc. Chil. Quim. 44 (1999) 435.
[15] M.A.S.D. Barros, E.A. Silva, P.A. Arroyo, C.R.G. Tavares, E.F. Sousa-Aguiar, Chem. Eng. Sci. 59 (2004) 5959.
[16] A. De Lucas, M. Uguina, I. Covián, L. Rodríguez, Ind. Eng. Chem. Res. 31 (1992) 2134.
[17] L.V.C. Rees, S. Chandrasekhar, Zeolites 13 (1993) 524.
[18] L.V.C. Rees, S. Chandrasekhar, Zeolites 13 (1993) 534.
[19] D. Akolekar, A. Chaffee, R.F. Howe, Zeolites 19 (1997) 359.
[20] V. Sanhueza, U. Kelm, R. Cid, J. Chem. Technol. Biotechnol. 74 (1999) 358.
[21] R. Aiello, C. Collela, R. Sersale, in: R.F. Gould (Ed.), Molecular Sieve Zeolites I, ACS Monograph, Washington, DC, 1971, pp. 51–52.
[22] V. Sanhueza, U. Kelm, R. Cid, J. Chem. Technol. Biotechnol. 78 (2003) 485.
[23] N. Murayama, H. Yamamoto, J. Shibata, J. Chem. Technol. Biotechnol. 77 (2002) 280.
[24] R. Juan, S. Hernández, X. Querol, J.M. Andrés, M. Moreno, J. Chem. Technol. Biotechnol. 77 (2002) 299.
[25] B. Subotić, I. Šmit, O. Madžija, L. Sekovanić, Zeolites 2 (1982) 135.
[26] F. Farzaneh, M. Khatamian, M. Akbary, J. Sci. Ind. Res. Iran 1 (1989) 23.
[27] TOPAS, General profile and structure analysis software for powder diffraction data, V2.0, Bruker AXS, Karlsruhe, Germany, 2000.
[28] D. Kashciev, S. Kiyotaka, J. Chem. Phys. 109 (1998) 8530.
[29] C. Kosanović, B. Subotić, I. Šmit, L.J.A. Despotović, Croat. Chem. Acta 74 (2001) 195.
[30] M.M.J. Treacy, J.B. Higgins, R. von Ballmoos, Collection of Simulated XRD Powder Diffraction Patterns for Zeolites, fourth revised ed., Elsevier, Amsterdam, 2001, p. 460.
[31] L.B. McCusker, Ch. Baerlocher, R. Nawaz, Z. Kristallogr. 171 (1985) 281.
[32] S. Hansen, U. Håkansson, A.R. Landa-Canovas, L. Fälth, Zeolites 13 (1993) 276.
[33] X. Querol, N. Moreno, J.C. Umaña, A. Aluastey, E. Hernández, A. López-Soler, F. Plana, Int. J. Coal Geol. 50 (2002) 413.
[34] R.A. Young (Ed.), The Rietveld Method, Oxford University Press, New York, 1995.
[35] E.M. Flanigen, in: J.A. Rabo (Ed.), Zeolite Chemistry and Catalysis, ACS Monograph, Washington, DC, 1976, pp. 83, 86–100.
[36] H.J. Percival, J.F. Duncan, P.K. Foster, J. Am. Ceram. Soc. 57 (1974) 57.
[37] E.M. Flanigen, H. Khatami, H.A. Szymanski, Adv. Chem. Ser. 101 (1971) 201.
[38] G. Rodríguez-Fuentes, C. Lariot, R. Roque, J.C. Romero, Zeolites 375 (1985) 5.
[39] L. Fälth, in: R. Sersale, C. Collela, R. Aiello (Eds.), 5th International Zeolite Conference, Recent Progress Report and Discussions, Napoli, 1981, p. 45.
[40] A. Katović, B. Subotić, I. Šmit, L.J.A. Despotović, Zeolites 9 (1989) 45.
[41] X.S. Zhao, G.Q. Lu, H.Y. Zhu, J. Porous Mater. 4 (1997) 245.
[42] A. Katović, B. Subotić, I. Šmit, L.J.A. Despotović, Zeolites 10 (1990) 634.
[43] F. Ucum, Z. Naturforsch. 57 (2002) 281.
[44] G. Engelhardt, J. Felsche, P. Sieger, J. Am. Chem. Soc. 114 (1992) 1173.
[45] D.W. Breck, Zeolite Molecular Sieves, Structure, Chemistry and Use, John Wiley & Sons, New York, 1974, p. 23, 449, 553, 168.
[46] C. Covarrubias, R. Arriagada, J. Yánez, R. García, M.A.S.D. Barros, P. Arroyo, E.F. Sousa-Aguiar, J. Chem. Technol. Biotechnol. 80 (2005) 899.
[47] M.Y. Kiriukhin, K.D. Collins, Biophys. Chem. 99 (2002) 155.
[48] Ch. Baerlocher, W.M. Meier, D.H. Olson, Atlas of Zeolite Framework Types, fifth revised ed., Elsevier, Amsterdam, 2001, p. 302.
[49] J. García-Martinez, D. Cazorla-Amoros, A. Linares-Solano, in: K.K. Unger, G. Kreysa, J.P. Baselt (Eds.), Studies in Surface Science and Catalysis. Characterization of Porous Solids, Elsevier, Amsterdam, 2002, p. 438.